Article:
Yang, J (2020) Computational Fluid Dynamics Studies on the Induction Period of Crude Oil Fouling in a Heat Exchanger Tube. International Journal of Heat and Mass Transfer, 159. 120129. ISSN 0017-9310

https://doi.org/10.1016/j.ijheatmasstransfer.2020.120129

Computational Fluid Dynamics Studies on the Induction Period of Crude Oil Fouling in a Heat Exchanger Tube

Junfeng Yang[a]

[a]School of Mechanical Engineering, University of Leeds, UK

Email Address: J.Yang@leeds.ac.uk

Colloquium for the research topic: Transport Phenomena and Fluid Mechanics

Abstract: Fouling impairs the hydrodynamic and thermodynamic performance of crude oil pre-heat train exchangers in refineries. The very early stage of fouling, so-called induction period, containing inappreciable levels of fouling is poorly understood due to a lack of experimental data. To better understand this period and seek potential fouling mitigation strategies, a model is implemented in a computational fluid dynamics (CFD) code, which accounts for chemical reaction- and precipitation-driven fouling, turbulent flow, and ageing in a heat exchanger tube. Three-dimensional CFD simulations are carried out under various operating conditions to gauge the relative importance of the two fouling mechanisms, and provide direct predictions of deposition rates. The interaction between chemical and precipitation fouling processes is characterized using an "interference factor", introduced to evaluate the extent of suppression of the chemical mechanism and enhancement of precipitation. The results provide insights into the interaction of key mechanisms during the induction period (up to three seconds flow time) of fouling in crude oil heat exchangers and possible strategies for prolonging this near nil-fouling period.

Keywords: crude oil fouling, precipitation, heterogeneous auto-oxidation, computational fluid dynamics.

Nomenclature

a	material-specific constant	[-]
A	pre-exponential factor for chemical reaction fouling	[Lmol-1s-1]
A	pre-exponential factor for aging model	[s-1]
B	constant value for ageing model	[-]
C	phase volume fraction or species concentration	[-]
Ca	Capillary number	[-]
d	asphaltenes phase mole fraction	[-]
D	pipe diameter	[m]
Dd	deposit diffusion coefficient	[m2s-1]
Ds	inverse of diffusion coefficient	[m2-s]
e	mathematical constant 2.71828	[-]
E	activation energy	[kJmol-1]
H	channel height	[m]
J	the mass flux from the oil phase to fouling phase	[kg/m2]
k	reaction rate constant	[Lmol-1s-1]
kt	ageing rate constant	[s-1]
K	equilibrium coefficient	[-]
K0	equilibrium constant at precipitation temperature	[-]
L	channel/pipe length	[m]

Lx	number of moles present for each phase	[mol]
M	molecular weight	[gmol-1]
n	normal vector	[-]
m, n, l	reaction order for reactant 1, 2, precursor	[-]
p	pressure	[Pa]
Pe	Peclet number	[-]
Pr	Prandtl number	[-]
r	reaction rate	[molL-1s-1]
R	universal gas constant	[-]
Re	Reynolds number	[-]
t	time	[s]
T	temperature	[K]
Tin	inlet flow temperature	[K]
Tp	precipitation temperature	[K]
Twall	wall surface temperature	[K]
u	velocity vector	[-]
V	velocity	[ms-1]
Vd	volume of deposit	[m3]
Vt	volume of channel	[m3]
x	horizontal coordinate	[-]

y_0	youth factor	[-]
z	vertical coordinate	[-]
β	thermocapillarity term	[K-1]
χ	weight fraction of each component of the mixture	[-]
$\dot{r}$	local shear rate	[s-1]
η	dimensionless function	[-]
λ	thermal conductivity of foulant	[Wm-1K-1]
λ_0	thermal conductivity for freshly deposit material	[Wm-1K-1]
λ_∞	the maximum value of thermal conductivity	[Wm-1K-1]
μ	viscosity	[Pas]
μ_0	viscosity of fresh foulant material	[Pas]
ρ	density	[kgm3]
σ	interfacial tension between oil phase and asphaltenes phase	[Nm-1]
τ	shear stress	[Pa]
ΔH_p	precipitation enthalpy	[kJmol-1]
θ	characteristic time for the formation of polyaromatic structure in the fouling layer	[s]
Θ	non-dimensional parameter that depends on Lx	[-]
ξ	structure parameter	[-]

Subscripts

0	initial	[-]
b	bulk	[-]
d	deposit	[-]
i	ith component	[-]
r1	reactant 1	[-]
r2	reactant 2	[-]

Abbreviation

2D	two-dimensional
3D	three-dimensional
CFD	Computational Fluid Dynamics
DNS	Direct Numerical Simulation
LES	Large Eddy Simulation
N-S	Navier-Stokes
RANS	Reynolds-averaged Navier–Stokes
VOF	Volume-of-fluid
PHT	Preheat Train
SAFT	Statistical Associating Fluid Theory
EOS	Equation of State

1. Introduction

Fouling in crude oil pre-heat trains impairs the thermodynamic and hydrodynamic efficiency of most oil refineries, but no elegant solutions to prevent it have been developed yet. Fouling involves complex chemical and physical mechanisms, including chemical reactions (notably auto-oxidation, precursor formation, crystallization, agglomeration and corrosion), sedimentation, and bio-fouling[1]. Once the foulant precursors have been produced, they eventually agglomerate and form wall deposits, which undergo rheological changes due to various thermal and physico-chemical factors, generally causing them to harden[2]. A fouled heat exchanger can be 'revived' by, for instance, mechanical cleaning, and addition of anti-fouling chemical additives, but all of these treatments inevitably increase costs.

Over the past few decades, intense efforts[3-14] have been made to address the fouling process in industrial crude oil heat exchangers, frequently involving experimental explorations of correlations between fouling rates physical factors under varying operating conditions. In early studies, it was generally assumed that the net fouling rate equals the deposition rate minus the removal rate[4]. However, Crittenden *et al*. (1979)[5] proposed a transport-reaction model for predicting deposition rates, in which chemical reactions and the transport of fouling precursors to and from the heated surface were considered. In addition, Epstein (1983)[1] identified five possible crude oil fouling mechanisms, and five sequential events. The cited model by Crittenden *et al*. (1979) was revised by Crittenden *et al*. (1987)[6] and Epstein (1994)[7], and further simplified by Yeap *et al*. (2004)[8] to a function of groups of turbulent flow parameters with a removal term. Based on data from coking experiments Ebert and Panchal (1995)[9] introduced a "threshold fouling" model, which has been further developed by Polley *et al*. (2002)[10] and Nasr and Givi (2006)[11] to improve the accuracy of the modeling for various crude oils. Shetty *et al* (2016)[12] proposed an improved threshold fouling model in which effective film temperature was introduced to capture the effect of bulk temperature variations. This improved model shows accurate prediction on the initial fouling rates against the experiments.

More recently, artificial neural network-based[13] and comprehensive shell-tube heat exchanger[14] models have also been developed and applied to model the fouling performance of heat exchanger networks of refinery plants. The threshold model is relatively simple to implement, and hence is widely

used. However, Yeap (2004)[8] evaluated several threshold fouling models and found that although they provide reasonable fits with data from laboratory experiments, they lead to poor predictions of fouling in industrial conditions. This is presumably due to weaknesses in the physical and chemical foundations of the models. Typically, for instance, the complex chemical kinetics and turbulence are lumped into a global reaction rate in a deposition term and shear stress in a removal term, respectively. The lumping simplifies the problem, but potentially important interactions and effects are lost. In addition, it is not clear which degree of the interfacial shear stress should form an input into the model. These two parameters strongly influence fouling evolution, and thus must be treated rigorously.

Thus, the fundamental physical and chemical processes underlying fouling require further elucidation. To improve our understanding, detailed *in situ* measurements of the intermediate species involved in the chemical reactions and local shear rates would be extremely helpful. However, characterizing the reactions would also be extremely challenging because the composition of crude oil is highly complex, and its oxidation reactions might involve hundreds or even thousands of intermediate species. Measurement of shear stresses in turbulent multiphase flows is also extremely challenging with current equipment. Thus, continuum-based Computational Fluid Dynamics (CFD), which has proven suitability for deepening insights into multiphase transfer processes, is being increasingly used to elucidate fouling processes in crude oil heat exchangers. Of course, this too is challenging, because the fouling involves interactions of multiple components moving in multiple phases in highly turbulent conditions, hence the models still need to be highly sophisticated.

To resolve the fluid motion across the full ranges of spatial and temporal scales, ideally Direct Numerical Simulation (DNS) should be applied, i.e. the Navier-Stokes equations should be solved without recourse to turbulence modelling. In order to achieve this, the computational grid must be sufficiently fine to resolve the flow down to the Kolmogorov scale, which depends on the average rate of energy dissipation per unit mass and kinematic viscosity. However, the computational cost of DNS is prohibitively expensive for typical industrial applications (where the crude oil has a water-like viscosity under the operating temperature above 500 K, and thus the Reynolds number, *Re*, of flows generally exceeds $O(10)^4$). Another approach involves the numerical solution of the Reynolds-

averaged (or time-averaged) N-S (RANS) equations together with an additional turbulence model, e.g. k-ε or k-ω models. RANS-based modelling allows the use of rather coarse grids, and thus greatly reduces the required computational costs, but only provides averaged fields, with no details of turbulent fluctuation. A further option is to use a Large Eddy Simulation (LES) approach to resolve the largest structures in the flow field, and account for sub-grid scale eddies using appropriate models. This methodology, which is implemented in this paper, provides a satisfactory compromise predictive accuracy and computational costs.

The fouling deposit-oil interface must also be captured or tracked, ideally, by using a dynamic mesh which follows the interfacial motion. To this end, Volume of Fluid (VOF) and Level-set methodologies have been employed in the literature, with the former being more suitable than the latter for capturing interfaces in terms of mass conservation[15]. Hence, interface-capturing is performed using a VOF approach in this paper.

In order to perform numerical simulations of industrial-scale fouling in PHT heat exchangers, which are typically 5-10 m long, large high-performance computing resources are required that are concomitant with the computational costs. Furthermore, fouling data obtained from refineries indicate that a deposit begins to form after continuous operation for several hundred hours, and accumulation continues until the heat-exchanger is taken off-line several months after the start of operation. Clearly, fouling simulations over these time-scales are computationally prohibitively expensive.

To overcome this obstacle, a possible approach is to solve non-dimensionalized NS equations first, then scale back the generalized results to practical dimensions. This approach was applied by Sileri (2009)[16] for simulating the laminar two-phase crude oil/foulant flows, taking into account asphaltenes precipitation and ageing. The non-dimensionalized results indicated that the Reynolds and capillary numbers govern the evolution of the flowing fouling layer. However, these results poorly reflect phenomena in real heat- exchangers in which the flow conditions are invariably turbulent. Another strategy involves simulating the flow in a segment of the heat-exchanger. Such an approach was employed by Bayat *et al*. (2012)[17] who simulated fouling in an axisymmetric 0.5 m long tube, accounting for turbulence by solving the RANS equations with k-ω transport equations. They used

two-lumped surface reactions and a species diffusion model to simulate fouling formation, deposition and ageing processes. Taking advantage of the much smaller number of computing cells in two-dimensional (2D) simulations, they investigated the accumulation of the fouling layer over 2000 hours of operating time. Although the fouling resistance was largely over-predicted during the induction periods, the 2D results confirmed the potential utility of CFD for simulating crude-oil fouling over long operating times. Tavakkoli *et al.* (2017)[18] developed a numerical tool based on Lattice-Boltzmann Method (LBM) to simulate the asphaltene deposition in a porous media. The predicted deposition rate was validated against the experimental data obtained from a microfluidic device, indicating that LBM is an efficient and alternative tool for simulating the crude oil fouling process. Loyola-Fuentes *et al.* (2018)[19] conducted the parametric fitting of fouling resistance on the reconciled mass flow rate and outlet temperature of heat exchangers. This simply fouling model was then employed to simulate the dynamic fouling process in a heat exchanger network. Although showing accurate prediction on fouling resistance, the model is not fully predictive since one requires, in advance, values of mass flow rate and outlet temperature that vary significantly from one refinery to another. Emani *et al.* (2019)[20] performed 3D discrete phase-CFD simulations of asphaltenes particles deposition using RANS model to investigate the effect of various forces on the rate of deposition of asphaltenes in a multi-pass shell and tube heat exchanger. Maddahian et al. (2020)[21] simulated asphaltene deposition and the fouling layer growth in a cylindrical tube using the multi-fluid approach. In which asphaltene deposition was simply treated as Arrhenius-type attachment rate. And the fouling layer growth was assumed to be a solidification process in a single-phase flow. Ishiyama *et al.* (2020)[22] recently updated the temperature field plot method (TFPM) by adding a simple deposit ageing model, which allows to investigate the impact of aged fouling on pressure drop in the preheat train heat exchangers. Rammerstorfer *et al.* (2020)[23] examined various existing fouling models (chemical reaction, corrosion and asphaltene precipitation), and found the effects of velocity and temperature on fouling rates should be accurately described in the adsorption-based fouling models regardless the fouling routes.

To achieve appreciable levels of fouling, most literature focus on the fouling process over a relatively long time scale (weeks or months)[24]. Valuable fouling data in industrial heat exchangers

were obtained and fouling rate models were derived. However, there are comparatively few literature reports investigating the early stage of fouling (so-called induction period), in which no significant fouling is observed when a new or clean heat exchanger is commissioned[25]. The induction period can last from few seconds to several hours, days, weeks, and even months, depending on the media and conditions[26,27]. Due to a lack of measureable experimental data on the fouling rate and the complexity of fouling behavior, a substantial understanding on the induction period remains elusive, and current experimental techniques have not yet proved to be sufficient for their identification. Yang *et al.* (2012)[28] examined the experimental data on fractional surface coverage of heat exchanger and proposed a simple lumped parameter model for predicting the induction process. This model was able to reasonably capture the fouling process from the start of the induction period up to the steady fouling rate stage. Yang *et al.* (2012)[28] also commented that the importance of the induction period should not be underestimated. A good quantitative knowledge of induction period provides possible strategies for prolonging this near nil-fouling period, and hence higher thermal efficiency of heat exchangers.

In a previous paper[29], we developed a comprehensive fouling model, which accounted for the thermophysical properties of crude-oil and asphaltenes phases, chemical- and phase-separation-driven fouling, as well as deposit aging; this model permitted the evaluation of the relative contributions of the fouling mechanisms to the overall fouling rate. Using this model, 3D LES as performed in a single tube to study the effects of wall surface temperature and bulk velocity on fouling deposition rates. We focused on the early stage of fouling, and the local phase transfer occurring close the inlet-end of heat exchanger. Our results indicated that the rate of chemical reaction-driven fouling is much larger than that associated with asphaltenes precipitation. Interestingly, we also found temperature ranges over which the rate of chemical reaction-driven fouling was reduced while that of asphaltenes precipitation was enhanced[30]. Although 3D CFD modelling can give accurate prediction on fouling process, it is computationally expensive when dealing with long timescale fouling in industrial heat exchangers. Hence, it is more appropriate to investigate the fouling during the induction period (several seconds flow time) and discover the fundamental understanding on the fouling routes using the current 3D CFD technique.

The objective of the present study is to extend our previous work to gain deeper insights into the interactions between the two fouling mechanisms during the induction period over a wide range of operating conditions through CFD simulations. A measure of the "interference" between the two mechanisms is introduced and the results are used to formulate possible strategies for fouling mitigation.

The rest of this paper is organized as follows. In Section 2, we present the details of our model. A discussion of our numerical results is provided in Section 3. Finally, Section 4 is devoted to concluding remarks.

2. Mathematical models

2.1 Governing Equations

The crude-oil fouling was treated as a multi-component, multi-phase, heat and mass transfer process, with both the oil and foulant phases treated as incompressible immiscible fluids. In the Finite Volume Method framework, the governing equations consist of two continuity equations, Eqs. (1) and (2) for oil and foulant phases, respectively, and a single set of momentum and energy equations, Eqs. (3) and (4), respectively):

$$\frac{\partial}{\partial t}(\alpha_o \rho_o) + \nabla \cdot (\alpha_o \rho_o \mathbf{u}_o) = S_{Mo} \quad \textbf{(1)}$$

$$\frac{\partial}{\partial t}(\alpha_f \rho_f) + \nabla \cdot (\alpha_f \rho_f \mathbf{u}_f) = S_{Mf} \quad \textbf{(2)}$$

$$\frac{\partial}{\partial t}(\rho \mathbf{u}) + \nabla \cdot (\rho \mathbf{u}\mathbf{u}) = -\nabla p + \nabla \cdot (\mu(\nabla \mathbf{u} + \nabla \mathbf{u}^{\mathbf{T}})) + \rho \mathbf{g} + F_{vol} \quad \textbf{(3)}$$

$$\frac{\partial}{\partial t}(\rho h_s) + \nabla \cdot \left(\mathbf{u}(\rho h_s + p)\right) = \nabla \cdot \left(\lambda \nabla T - \nabla \cdot \left[\sum_{q=1}^{n} h_{s,q} \left(\rho D_{m,q} \nabla Y_q\right) \right] \right) + S_h \quad \textbf{(4)}$$

where subscripts *f* and *o* denote the foulant and oil phases, respectively, α, ρ and $\mathbf{u}$ are the volume fraction, density and velocity of each phase, respectively, p and $\boldsymbol{g}$ indicate pressure and gravitational acceleration respectively, and S_M is the mass source term for each phase due to the mass transfer process, e.g. chemical reaction or precipitation. Here, $\frac{\partial}{\partial t}$ denotes the partial derivative with respect to time, and ∇ the gradient operator. The physical properties of multiphase system, density, ρ, viscosity,

μ, and thermal conductivity, λ, are volume-fraction-averaged variables[31] calculated using the following equations:

$$\rho = \alpha_f \rho_f + \alpha_o \rho_o \quad \textbf{(5)}$$

$$\mu = \alpha_f \mu_f + \alpha_o \mu_o \quad \textbf{(6)}$$

$$\lambda = \alpha_f \lambda_f + \alpha_o \lambda_o \quad \textbf{(7)}$$

The above properties for fouling layer, e.g. μ_f and λ_f, are usually governed by the ageing process that will be described in Section 2.6. The surface tension force resulting from an imbalance between cohesive forces and adhesive force among oil molecular and foulant molecular at the interface of oil and fouling phases was modelled using the Continuum Surface Force (CSF)[32] method and was taken into account via the source term, F_{vol}, in the momentum equation:

$$F_{vol} = \sigma_{fo} \frac{\rho \kappa_f \nabla \alpha_f}{\frac{1}{2}(\rho_f + \rho_o)} \quad \textbf{(8)}$$

where σ_{fo} indicates the interfacial tension coefficient, taking the value of 0.03 N/m for oil and fouling phases, and κ represents the curvature defined by the divergence of the unit normal. Equations (3) and (4) are solved throughout the domain, and the resulting velocity and temperature fields are shared between the oil and fouling phases (see below). As the crude oil-foulant system is regarded as incompressible in the present model, the pressure work is excluded from the model; viscous heating effects are also neglected when solving the energy equation (Eq. (4)). The second and third terms on the right-hand-side of Eq. (4) written as $\lambda \nabla T$ and $\nabla \cdot \left[\sum_{q=1}^{n} h_{s,q} \left(\rho D_{m,q} \nabla Y_q\right)\right]$, represent the energy transfer due to conduction and species diffusion, respectively. The sensible enthalpy, h_s, and temperature, T, are determined by the microscopic motion of a large number of molecules, and thus follow mass-averaged expressions[31]:

$$h_s = \frac{\alpha_o \rho_o h_{s,o} + \alpha_f \rho_f h_{s,f}}{\alpha_o \rho_o + \alpha_f \rho_f} \quad \textbf{(9)}$$

$$T = \frac{\alpha_o \rho_o T_o + \alpha_f \rho_f T_f}{\alpha_o \rho_o + \alpha_f \rho_f} \quad \textbf{(10)}$$

For each phase, $h_{s,o}$ and $h_{s,f}$ are defined as the sum of species enthalpy, which is based on the specific heat (C_p) of that species and the shared temperature (T). The variables $h_{s,o}$ and $h_{s,f}$ have a similar formulation, e.g. (for $h_{s,f}$):

$$h_{s,f} = \sum_{q=1}^{m} h_{s,f,q} Y_q = \sum_{q=1}^{m} Y_q \left(\int_{T_{ref}}^{T} C_p \, dT \right) \quad \textbf{(11)}$$

where $h_{s,f,q}$ is the enthalpy of the q^{th} species in the foulant phase, Y_q is the concentration of the q^{th} species and m is the total species number in the considered phase.

The source term in energy equation, S_h, includes the heat release due to chemical reaction written as:

$$S_h = \sum_{q=1}^{n} \frac{h_q^0}{M_{w,q}} R_q \quad \textbf{(12)}$$

where h_q^0 , $M_{w,q}$ and R_q are the enthalpy formation, molecular weight and volumetric rate of creation of the q^{th} species, respectively. To track the interface between the oil and fouling phases, the following continuity equation for the volume fraction of the fouling phase, α_f, is solved:

$$\frac{\partial \alpha_f}{\partial x} + \mathbf{u_f} \cdot \nabla \alpha_f = 0 \quad \textbf{(13)}$$

The volume fraction of the oil phase (the primary phase), α_o is then simply determined as 1 - α_f.

The concentration of each species, Y, can be predicted by solving the convection-diffusion equation using Fick's law. Assuming that mass diffusion of a species is driven solely by concentration gradients, the conservation equation for the q^{th} species is written as:

$$\frac{\partial}{\partial t}(\rho Y_q) + \nabla \cdot (\rho Y_q \mathbf{u}) = \nabla \cdot [\rho D_{m,q} \nabla Y_q] - R_q \quad \textbf{(14)}$$

where D_m is the mass diffusion coefficient, taking the value of 10^{-7} m^2/s for all the species. R_q is the net production rate of the q^{th} species via chemical reactions, formulated as the sum of all relevant Arrhenius reaction rates multiplied by the species' molecular weight.

To predict the transient turbulent flow field accurately, the LES approach is employed and Eqs. (1) -(4) are filtered as follows:

$$\frac{\partial}{\partial t}(\alpha_o \rho_o) + \sum_{i=1}^{3} \frac{\partial}{\partial x_i}(\alpha_o \rho_o \bar{u}_{oi}) = S_{Mo} \quad \textbf{(15)}$$

$$\frac{\partial}{\partial t}(\alpha_f \rho_f) + \sum_{i=1}^{3} \frac{\partial}{\partial x_i}(\alpha_f \rho_f \bar{u}_{fi}) = S_{Mf} \quad \textbf{(16)}$$

$$\frac{\partial}{\partial t}(\rho\bar{u}_i) + \sum_{j=1}^{3}\frac{\partial}{\partial x_j}(\rho\bar{u}_i\bar{u}_j) = -\sum_{i=1}^{3}\frac{\partial\bar{p}}{\partial x_i} + \sum_{j=1}^{3}\frac{\partial}{\partial x_j}\left[\mu\left(\frac{\partial\bar{u}_j}{\partial x_i} + \frac{\partial\bar{u}_i}{\partial x_j} - \frac{2}{3}\delta_{ij}\sum_{k=1}^{3}\frac{\partial\bar{u}_k}{\partial x_k}\right)\right] - \sum_{j=1}^{3}\frac{\partial\tau_{ij}}{\partial x_j} + \rho g + F_{vol} \quad \textbf{(17)}$$

$$\frac{\partial}{\partial t}(\rho\overline{h_s}) + \sum_{i=1}^{3}\frac{\partial}{\partial x_i}(\rho\bar{u}_i\overline{h_s}) - \frac{\partial\bar{p}}{\partial t} - \bar{u}_j\sum_{i=1}^{3}\frac{\partial\bar{p}}{\partial x_i} - \sum_{i=1}^{3}\frac{\partial}{\partial x_i}\left(\lambda\frac{\partial\bar{T}}{\partial x_i}\right) = -\sum_{j=1}^{3}\frac{\partial}{\partial x_j}\left[\rho\left(\overline{u_\iota h_s} + \bar{u}_i\overline{h_s}\right)\right] + S_h \quad \textbf{(18)}$$

where $\bar{p}$, $\bar{u}$, $\bar{T}$ and $\overline{h_s}$ are the filtered pressure, velocity, temperature and sensible enthalpy field, respectively, while *i*, *j* and *k* are the vector components in the i^{th}, j^{th} and k^{th} directions, respectively. On the right-hand-side of the filtered momentum equation (Eq. 17), the unknown term,τ_{ij}, is the sub-grid scale stress defined as $\tau_{ij} = \rho\overline{u_\iota u_J} + \rho\bar{u}_i\bar{u}_j$, and can be further simplified for incompressible fluids as $\tau_{ij} = -2\mu_t\bar{S}_{ij}$. Here, $\bar{S}_{ij}$ is the rate-of-strain tensor for the resolved scales defined by:

$$\bar{S}_{ij} = \frac{1}{2}\left(\frac{\partial\bar{u}_j}{\partial x_i} + \frac{\partial\bar{u}_i}{\partial x_j}\right) \quad \textbf{(19)}$$

To close this problem, the Smagorinsky–Lilly[33] model is employed to predict the sub-grid scale eddy viscosity, μ_t:

$$\mu_t = \rho L_s^2|\bar{S}| \quad \textbf{(20)}$$

The standard Smagorinsky-model cannot produce the correct asymptotic behavior for μ_t, in the near-wall region ($\mu_t \sim y^3$). Limiting μ_t with the mixing length provides an *ad hoc* approach to bring the asymptotic behavior closer to the behavior of real systems. Therefore, the present work formulates μ_t using Smagorinsky-Lilly theory together with a Prandtl mixing length model:

$$\mu_t = \rho L_s^2|\bar{S}| = \rho[\min(\kappa_{von}d,\ C_s\Delta)]^2\sqrt{2\bar{S}_{ij}\bar{S}_{ij}} \quad \textbf{(21)}$$

where κ_{von} is the von Karman constant (0.41), *d* is the distance to the closest wall, C_s is the Smagorinsky constant (0.1 adopted herein), and Δ is the local grid size. The min-function selects the Prandtl mixing length model close to the wall boundary, but switches to the Smagorinsky model away from the wall.

In the filtered energy equation (Eq. 18), the term $\rho\left(\overline{u_i h_s} + \bar{u}_i \overline{h_s}\right)$, designated the sub-grid enthalpy flux, was modelled by the gradient transport hypothesis:

$$\rho\left(\overline{u_i h_s} + \bar{u}_i \overline{h_s}\right) = \frac{\mu_t C_p}{Pr_t} \frac{\partial \bar{T}}{\partial x_i} \quad \textbf{(22)}$$

where Pr_t is the sub-grid turbulent Prandtl number (0.85) and C_p is the heat capacity.

The difference between the filtered and unfiltered governing equations is that the former includes the filter field ($\bar{u}, \bar{p}, \bar{T}$ *and* $\overline{h_s}$). In the CFD-based approach used in the simulations reported here, all of the above governing equations are discretized and solved simultaneously using the commercial code ANSYS Fluent[34] ver. 18.0.

2.2 Description of the Fouling Formation Routes

Real crude oil and fouling phases have very complex compositions (including saturates, aromatics, resins and asphaltenes)[35] that vary from one locality to another. Thus, they have highly heterogeneous thermophysical properties. To handle this heterogeneity, pseudo-component[36] and surrogate[29,37] models have been proposed, which assume that the properties of crude oil reflect those of its major hydrocarbon constituents and their volumetric proportions. In our previous work[29,37], the crude oil surrogate and foulant surrogate models have been developed to approximate the temperature-dependent liquid properties, e.g. viscosity and thermal conductivity, of crude oil and foulants, respectively. The dominant constituents of surrogate models are paraffin and aromatic hydrocarbons with carbon numbers ranging from C_6 to C_{24}, e.g. benzene, n-heptane, 1-methylnaphathalene and tetracosane. The properties of those constituents have been estimated using empirical methods and further used to calculate the surrogates' properties according to their volumetric ratios. Those properties were used in this work without modification. These dominant constituents constitute 90% of crude oil by mole fraction, and the remaining 10% is the asphaltenes component.

Apart from the surrogate models, the comprehensive fouling model includes a fouling formation model and ageing model, which are briefly described in the following section. Interested readers are referred to Refs. [29-30] for details.

2.3 Fouling Formation Routes

As already mentioned, five crude-oil fouling formation mechanisms have been identified in Ref. [1]. Two of them, sedimentation and bio-fouling, arising from impurities and microorganisms, were excluded in the present work since the crude oil and foulants were assumed to be organic mixtures of hydrocarbons[38], for which these processes are negligible. Corrosion fouling arising from the surface reaction on inner wall is not well understood and data for corrosion rate is scarce[38]. Thus, the presented simulations and discussion focus on the chemical reaction-based and physical precipitation fouling pathways (see Fig. 1). In chemical fouling it is assumed that the foulant precursors generated by auto-oxidation in which react to form agglomerates of insoluble foulant, while in precipitation it is assumed that soluble foulants (e.g. asphaltenes) become insoluble via phase-separation processes controlled by equilibrium. In general, the autoxidation only occurs when dissolved oxygen is present as well as certain types of unsaturated hydrocarbon. Although there is rare much oxygen molecular present in crude oil, the oxygenated compounds, e.g. dibenzofuran ($C_{12}H_8O$) which commonly present in the crudes, also favor the autoxidation as the reaction sites, C-O•, are created via the cleavage of C-O bond of the furanic ring under the high temperature conditions. Note that both fouling routes are regarded as essentially irreversible processes in the present model, despite experimental indications that asphaltenes precipitation is partially reversible under appropriate pressures[39].

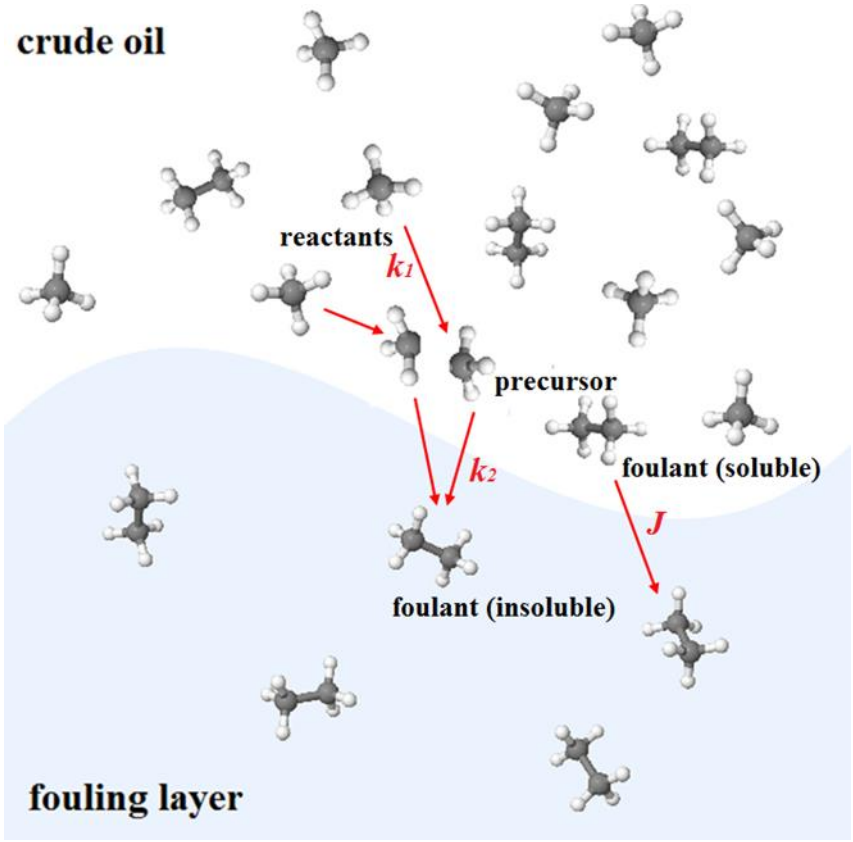

Figure 1 Schematic illustration of the formation of a fouling layer via chemical reaction and precipitation mechanisms in a multi-component asphaltenes-oil system.

2.4 Hydrocarbon Auto-oxidation Route

In an industrial PHT heat exchanger, the autoxidation of hydrocarbons was identified as one of the major sources of chemical reaction fouling occurring at moderate temperatures (T<650 K), where coking rarely occurs[40]. This may occur everywhere in the heat exchangers, e.g. bulk, boundary layers and wall deposits[41]. Due to the complex nature of crude oil and its reactions, a large numbers of species and reactions need to be identified to establish detailed kinetics of chemical fouling, which is beyond current measurement and kinetic modeling capabilities. However, the auto-oxidation of light hydrocarbons, e.g. indene[40,41] and kerosene-type[42] fuels have been widely studied because kerosene's results relate directly to jet fuel fouling, and indene usually is usually selected as the model compound readily forms the foulant precursors, i.e. poly-peroxide gums. The crude oil fouling in the present study was assumed following a kinetic scheme similar to those light hydrocarbons. Generally, the autoxidation is initiated by hydrogen atom abstraction caused by collisions between oil molecules and small radicals. The presence of fuel-bound oxygen allows hydrocarbon radicals to form hydroperoxides and polyperioxides, which are finally converted into foulant species via vinyl polymerization[38]. This general autoxidation scheme was lumped into two-step reactions (see Fig. 2): the initial generation of a soluble precursor (including initiation and propagation) followed by the formation of an insoluble foulant (so-called termination) as shown below:

$$\underset{\text{(soluble)}}{\textbf{Reactants}} \xrightarrow{r_1} \underset{\text{(sparingly soluble)}}{\textbf{Precursor}} \xrightarrow{r_2} \underset{\text{(insoluble)}}{\textbf{Foulant}}$$

Figure 2 Two-step reaction concept for chemical fouling route[39]

Here, r_1 and r_2 are the reaction rates for the first and second reactions, respectively:

$$r_1 = k_1 C_{r1}^m C_{r2}^n \quad \textbf{(23)}$$

$$r_2 = k_2 C_p^l \quad \textbf{(24)}$$

In the above expressions, C_{r1}, C_{r2} and C_p are the concentrations of reactants (oil components, hydroperoxides and polyperioxides) and precursors, respectively, while m, n, l are the orders of these species, to be 1.5, 0.5 and 1, respectively; k_1 and k_2 are reaction rate constants.

The reaction rates of indene oxidation have been derived through experiments in closed shaken flasks at both atmospheric and reduced pressures[41], and validated using higher pressure (at approximately 4 bar) laboratory-scale fouling apparatus in which the fouling resistance and deposition rates were measured in a heating tube filled with cycling indene/kerosene fluids[40]. In our previous work[29,30], the effect of pressure on the reaction rate was neglected and the reaction kinetics developed for low pressure conditions were applied to predict the fouling at high operating pressure without any adjustments. However, studies have revealed that asphaltenes oxidation is strongly (and positively) pressure-dependent: increasing the pressure from 4 bar to 20 bar at approximately 370 K may increase the reaction rate by up to 70%[43]. The operating pressure of industrial PHT heat exchangers is usually about 30 bar maximum with temperature 500-600 K. This pressure decreases down the PHT and is usually much lower at the hot end where the fouling is most problematic due to the competition between low pressure and high temperature. Thus, the reaction rate constants, k_1, k_2, applied here have the form specified by the temperature- and pressure-dependent Arrhenius equation:

$$k_{1,2} = A' \exp\left(-\frac{E}{RT}\right) \quad \textbf{(25)}$$

where A' is the pre-exponential factor, E is the activation energy, R is the universal gas constant, and T is the local temperature; A' and E are empirically determined, pressure-dependency parameters written as $A' = 0.0189\exp(0.356E)$ and $E = [11.3 \ln p + 5.19] + 134.6C5/C7$, respectively[43]. The ratio of heptanes asphaltene ($C7$) to pentane asphaltenes ($C5$) is used in Ref. [43] as the asphalt compositional parameter.

2.5 Asphaltenes Precipitation

Asphaltenes are compounds with high molecular weights that are insoluble in n-alkanes, but soluble in aromatic solvents. Heavy crude oil usually has a high volumetric percentage of dissolved asphaltenes, which may precipitate out due to fluctuations in temperature, pressure or composition. Numerous studies have explored asphaltenes solubility in crude oil at various temperatures and

pressures. Temperature has various, competing effects on its solubility. It was reported that its solubility in crude oil increases with temperature between 370 and 410 K, but may increase and decrease as temperature increases further[44-45]. That's because the π- and hydrogen-bonding that drive asphaltenes aggregation and precipitation become far weaker than covalent bonding between carbon atoms, and tend to break in the presence of solvent at higher temperatures[44]. However, the predominately alkane molecules, which have relatively high coefficient of thermal expansion, tend to expand, thereby reducing asphaltenes solubility[46]. Moreover, reductions in molecular viscosity at high temperature enhance molecular diffusion and thus accelerate aggregation[47]. At low temperatures, effects of thermal expansion and molecular diffusion are relatively minor compared to the bonding effect. Thus, asphaltenes has a smaller chance to aggregate, and exhibits higher solubility. As temperature increases further, the competition between asphaltenes solubility-enhancing factors (bonding forces) and solubility-suppressing factors (thermal expansion and diffusion) intensifies and its solubility may either decrease or increase depending on the relative strength of the factors. Both monotonic increases as well as increases followed by reductions in asphaltenes solubility have been reported in experimental and numerical studies[44-45,48-49].

To better understand asphaltenes phase behavior, various models have been developed in attempts to describe or predict experimental observations of asphaltenes precipitation and deposition. Two classes of these models can be distinguished: colloidal models (which assume that asphaltenes exist in the oil as solid particles dispersed in a resinous two-phase system) and thermodynamic models (which assume that asphaltenes is solvated by crude oil and phase separation occurs when the solvation power of oil is too poor)[50]. Thus, the critical chemical potential of resins is used to determine if the asphaltenes fraction is stable or not in colloidal models, while the volume fraction of soluble asphaltenes is estimated in thermodynamic models by phase equilibrium calculations, using for example regular solution, cubic- or SAFT-based Equation of State (EOS) approaches. Although these models reportedly provide reasonable predictions for limit conditions, none of them can consistently predict asphaltenes precipitation accurately. However, a modified regular solution method, so-called chemical equilibrium model[49], based on Gibbs free energy was developed to describe wax deposition on

the wall of pipelines. This model treats the asphaltenes deposition as a phase instability phenomenon and takes into account the phase equilibria, phase transitions, thermodynamics and fluid dynamics to quantify the amount of mass phase-separation in the oil. The mass flux from crude oil to fouling phases is based on Fick's law of diffusion:

$$J = -D_m\left(\frac{\rho\eta}{T}\frac{\partial T}{\partial \mathbf{n}}\right) \tag{26}$$

where D_m is the diffusion coefficient of the diffusing foulant species, ρ is the total density, and **n** is the normal vector to the wall; η is a dimensionless function written as:

$$\eta = \sum_{q=1}^{n}\eta_q\,, \quad \text{and} \quad \eta_q = \chi_q\frac{\left[T(1+\theta)^2\frac{\partial L_x}{\partial T} + \theta\frac{\Delta H_{Pq}}{RT}\right]K_q}{\left(1+\theta K_q\right)^2} \tag{27}$$

Here, χ_q, is the weight fraction of each component of the mixture, and θ is a parameter that depends on the number of moles, L_x, present for each phase. K_q is the phase equilibrium constant for the q^{th} component of the oil mixture. n is the total number of species in the system. $\Delta H_{Pq}$is the precipitation enthalpy the q^{th} component of the oil mixture, the value of 34.9 kJ/mol and 107.8 kJ/mol adopted herein for oil and asphaltenes[16], respective. Formulations for K_q, χ_q, θ and L_x are given and discussed elsewhere[16,29,51]. This chemical equilibrium model is consistent with experimental observations and has been implemented into a numerical model to predict the wax deposition in an industrial pipeline system[51]. It has also been incorporated into CFD code to investigate the evolution of crude oil fouling in heat exchangers by 2D DNS[16,30] and 3D LES[29-30] simulations. In contrast to the phase instability assumption, another group of thought is that asphaltenes deposition is kinetically driven, resulting from the reaction of asphaltenes and proposed a chemical kinetics for asphaltenes precipitation[52] similar to two-step reaction fouling scheme. A detailed description of kinetically driven model would be beyond the scope of this work, and so only the phase instability driven model used in the studies reported herein is described.

The above two-step reaction concept of indene autoxidation and chemical equilibrium model were used to represent the chemical fouling and asphaltenes precipitation routes, respectively, in this study. Note that Eqs. (23)-(27) indicate that these two routes are strongly influenced by the local temperature, temperature gradient and species concentration. Although different fouling mechanisms have been

identified and some interactions among them have been studied, e.g. interaction between crystallization and particulate fouling[53,54] and the mixed fouling (biological reactions, carbonate precipitation and particulate) involving biofilms[55,56], fouling route interactions in crude oil preheat trains have not been previously explored.

2.6 Aging Process

As previously mentioned, the exposure of the fouling layer to temperature and shear stresses over extended periods of time causes its molecular structure and liquid properties to change via a series of physico-chemical processes. The gel-like foulant layer eventually degrades to a hard material. During this ageing process, changes in the liquid properties of the foulant layer, such as its viscosity and thermal conductivity, alter the adhesion forces that bind it to the wall and hold it together as well as its heat transfer properties. This, in turn, affects the deposition and removal processes.

To describe the variation of asphaltenes properties (thermal conductivity, λ_f and viscosity, μ_f), the ageing models developed in previous work[29-30,57-58] are summarized briefly in Eq. (28):

$$\lambda_f = \lambda_f^{\infty} + \left[\lambda_f^{0} - \lambda_f^{\infty}\right] \times y_0 \times \exp(-k^t \times t)$$
$$\mu_f = \mu_{0,f}\left[1 + \frac{\frac{1}{\theta} - \exp(-t - 0.032)}{\alpha|\dot{\gamma}|}\right] \quad \textbf{(28)}$$

The impact of ageing on thermal conductivity can be modelled using the simple assumption that the foulant's thermal conductivity varies between the minimum value (λ_f^0) for fresh foulant and a maximum value (λ_f^{∞}) for a coke-like deposit. The ageing effect on viscosity is described by a rheological model for thixotropic substance, based on the ratio of the shear stress and shear rate. These properties of aged foulant (λ_f and μ_f) were taken into account in Eqs. (6)-(7) for calculating the averaged properties, λ and μ, of fluid, which were, in turn, used as inputs for the energy equations [Eqs. (4) and (18)] and momentum equations [Eqs. (3) and (17)].

In Eq. (28), y_0, k and t are the "youth" factor, temperature-dependent ageing rate constant, and lifetime of foulant, respectively; $\mu_{0,f}$, θ, α and $\dot{\gamma}$ are the viscosity of fresh foulant, ageing constants and local shear rate, respectively. Details of the mathematical deduction of aging models and the initial value of each parameter are given in Refs. [29-30, 57-58].

2.7 Numerical setup

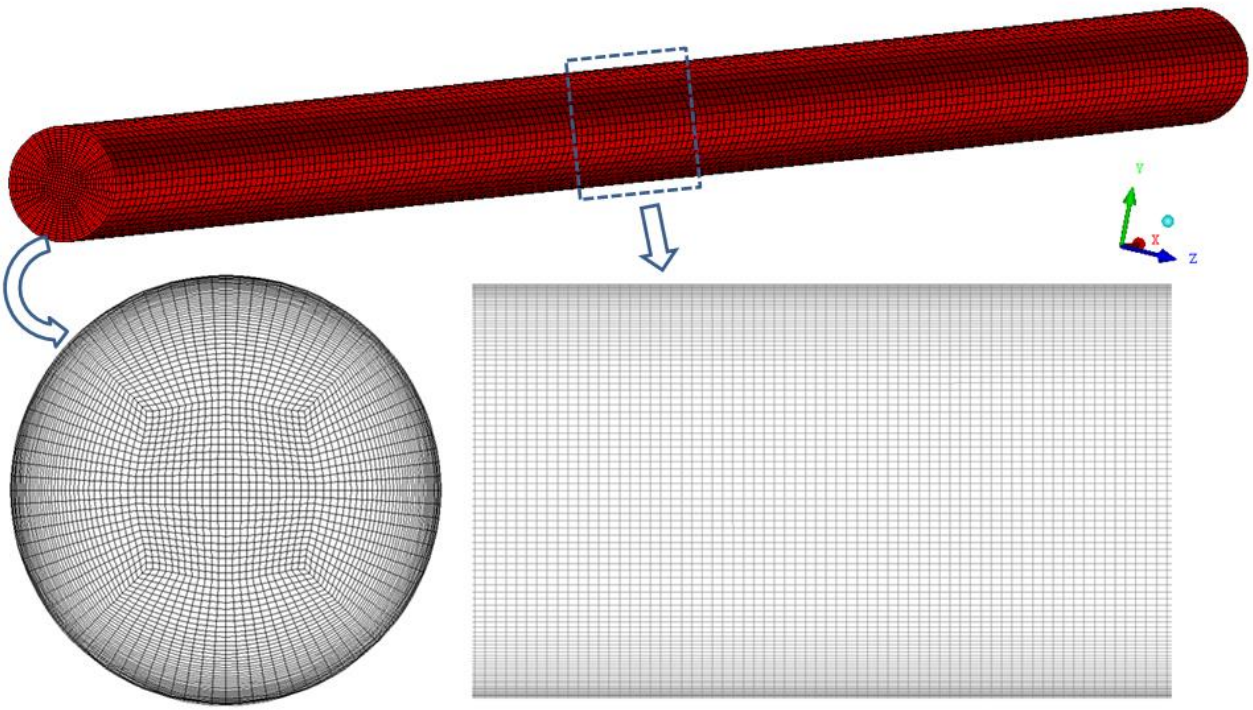

Figure 3 The computational domain, consisting of ~5 million unstructured hexahedral elements for a heat exchanger tube 0.5 m long with 0.02 m diameter.

A PHT heat exchanger is typically 5 to 10 m long. To reduce the computational time, a single tube 0.5 m long with 0.02 m diameter was selected to mimic the entire tube. Such a short tube may not allow full development of turbulent pipe flow. To overcome this shortcoming, periodic boundary condition[23] were used in a trial simulation to obtain fully-developed turbulent pipe flow, which was then applied as an initial velocity field for the final simulations.

A 3D computational domain (see Fig. 3), consisting of ~5 million unstructured hexadedral cells, was constructed using the commercial mesh generator ICEM CFD[59]. To resolve the fouling layer adjacent to the wall surface, mesh gradients (fine grids near the wall and coarse grids for the core region) were applied in the radial direction. A uniform grid size was used in the axial direction. The boundary conditions for the left and right ends were imposed as periodic conditions with constant pressure-gradient for RANS simulation, or velocity inlet/pressure outlet conditions for LES simulation. A no-slip condition was imposed on the wall, and a constant wall temperature was assumed for the thermal boundary condition. Operating conditions of an inlet stream (bulk velocity, V_b, 1m/s, temperature 474 K) entering a tube heat exchanger (tube wall temperature, T_w, 575 K, operating

pressure 30 bar) in Ref. [14], were adopted and varied ($0.25 < V_b < 1.5$ m/s; $525 < T_w < 625$ K) to evaluate the physical quantities across ranges of practical interest.

The simulation procedure consists of three separate runs (Fig. 4). First, a standard RANS k-ε simulation is run in a relatively coarse mesh with the periodic boundary condition, and crude oil containing 10 mol% asphaltenes flowing through the tube with no phase separation and ageing to obtain a steady, fully-developed turbulent field (see Figs. 4(a) and (d)) within a relatively short computational time. Second, interpolating the RANS velocity profile to a fine mesh (see Fig. 3) and adding the fluctuation components which were computed by synthesizing a divergence-free velocity-vector field from the summation of Fourier harmonics, with a switch to the LES Smagorinsky-Lily model, to produce fully-developed transient turbulent flow (see Figs. 4(b) and (e)). In the third run, the periodic boundary condition is switched to velocity inlet and pressure outlet for left and right ends, respectively; the initial velocity, turbulent kinetic energy and dissipation rate are interpolated, the VOF and fouling models are activated, allowing the evolution of the fouling layer to be tracked. All of the simulation results are collected and analyzed in this run. Figs. 4(c), (f) and (g) present the velocity profile for a particular case in which the third run with an initial fouling layer adjacent to the wall in the middle of tube is tested.

The aforementioned fouling models, including thermophysical properties, physical and chemical fouling routes and ageing model were incorporated into the commercial CFD solver ANSYS Fluent ver. 18.0 via a User Defined Function interface that produces the instantaneous source terms and temperature-dependent fluid properties for the governing equations.

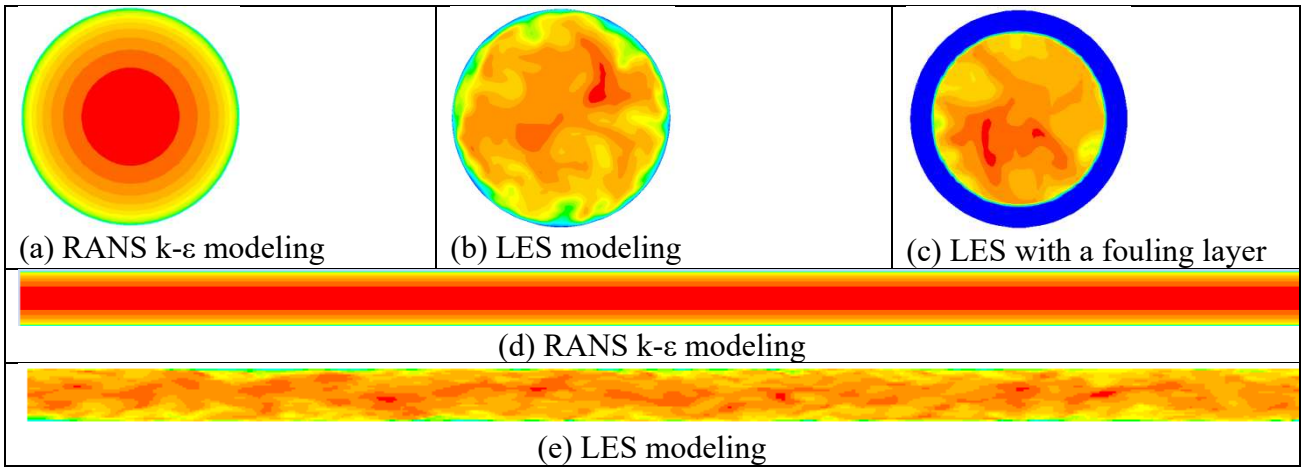

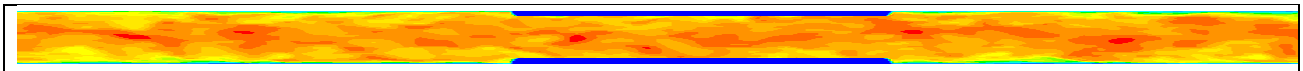

(f) LES with a fouling layer

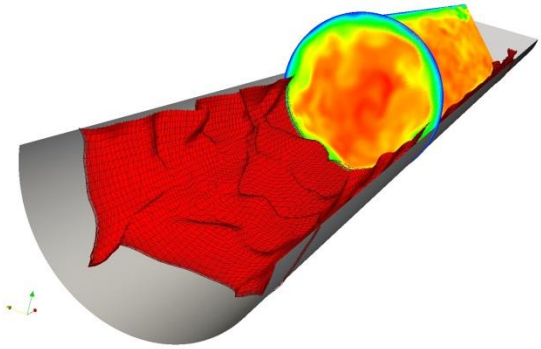

(g) iso-surface of fouling layer and velocity field obtained from LES modeling

0.0 0.25 0.5 0.75 1.0 [m/s]

color bar for fluid velocity

Figure 4 Cross-sectional views (longitudinal (a)-(c) and transverse (d)-(f)) of the velocity field obtained from three runs following the simulation procedure (see text for details).

In a turbulent oil/fouling multiphase system, the turbulence dynamics on the two sides of the interface differ, and the interaction between the turbulence structure and interface strongly influences the evolution of the fouling layer, especially the interface deformation. Usually, the LES model needs to be solved together with a prescribed turbulence damping function that provides a source term for the specific dissipation rate to avoid unrealistic production of turbulent kinetic energy in the primary fluid due to the relatively high strain rates on the other side of interface. In the present work, a sufficiently fine mesh was used adjacent to the wall region where the oil/fouling interface is usually located to make the effect of sub-grid turbulence insignificant. Therefore, no turbulence damping function at the interface was used here.

The pressure-velocity coupling was handled by the Semi-implicit Method for Pressure-linked Equation (SIMPLE) algorithm, while Pressure Implicit with Splitting Operator (PRESTO) and bounded central differencing schemes were used as the discretization methods for pressure and velocity, respectively. The High Resolution Interface Capturing (HRIC) scheme was chosen for VOF and second order upwind scheme for other convection terms, energy and species. The second order implicit method was used to advance the solution in time. To ensure accuracy, the global Courant number was kept to less than 0.25 by choosing a fixed time step of 0.0001s and a maximum number

of 20 iterations for each time step. All of the simulations were conducted on a HP-Z820 24-core 3.4 GHz workstation run in parallel.

3. Modeling Results and Discussion

Factors that influence fouling processes (including wall surface temperature, bulk velocity, bulk temperature and crude type) have been widely studied[3]. Generally, high surface temperature and "heavy" crudes are associated with strong fouling rates. However, both acceleration and deceleration of the fouling rate have been reported at high bulk temperatures due to the complex relationship between asphaltenes solubility and temperature as discussed in Section 2.5. In addition, the fouling rate may either increase or decrease as the bulk velocity increases, depending on the predominant fouling mechanism (i.e. whether it is largely governed by chemical reactions or mass-transfer)[3]. Thus, these factors have highly complex, interactive effects on the fouling route(s). Moreover, fouling involves various mechanisms, any pair of which may have synergistic or antagonistic effects. However, very few studies have assessed interactions between the mechanisms, even though better understanding of the interactions could be helpful for developing effective mitigation strategies. Thus, the present study addresses chemical and precipitation fouling under various operating conditions, and evaluates their interactions by assessing effects of including them individually and together in simulations. Throughout the following discussion, fouling rate was calculated taking into account the mass variation of insoluble asphaltenes occurring everywhere in the heat exchangers. This overall fouling rate considers not only the foulant formed in the bulk and wall region, but also those diffusing and adhering to the wall. The mass variation of fouling material advected out of the tube was referred to the removal rate.

3.1 Effects of Wall Temperature and Bulk Velocity

The effect of varying the wall temperature on the predicted foulant concentration in bulk (the mass of foulant phases per unit volume in the computational domain) and foulant formation rate (the volume-averaged mass transfer rate from oil-phase to foulant-phase) driven by asphaltenes precipitation route at a fixed bulk velocity ($Re = \frac{\text{bulk density} \times \text{bulk velocity} \times \text{pipe diameter}}{\text{bulk viscosity}} = 15000$), is

illustrated in Figs. 5(a) and (b), respectively. Clearly, increasing the wall surface temperature accelerates foulant formation; the averaged formation rate is approximately twice as high at 625K than at 525 K. The effect of varying the bulk velocity on the foulant concentration and formation rate over the entire fluid domain was also investigated by varying *Re* at constant wall temperature (575 K); this is displayed in Figs. 5(c) and (d). As the bulk velocity increases from 0.25 to 1.5 m/s, through an increase in *Re* from *Re*=15000 to *Re*=90000, the foulant formation rate is approximately halved. The foulant concentration (Fig. 5(c)) at *Re* > 15000 reaches an asymptote after 1 s, which indicates the fouling deposition rate (Fig. 5(d)) and remove rate become equal. The contours for instantaneous in-tube temperature and fouling deposition rate are also illustrated for different wall temperatures in Figure 6, which shows that fouling deposition rates are high in the high-temperature regions near the wall; hence most foulants form in the thermal boundary layer.

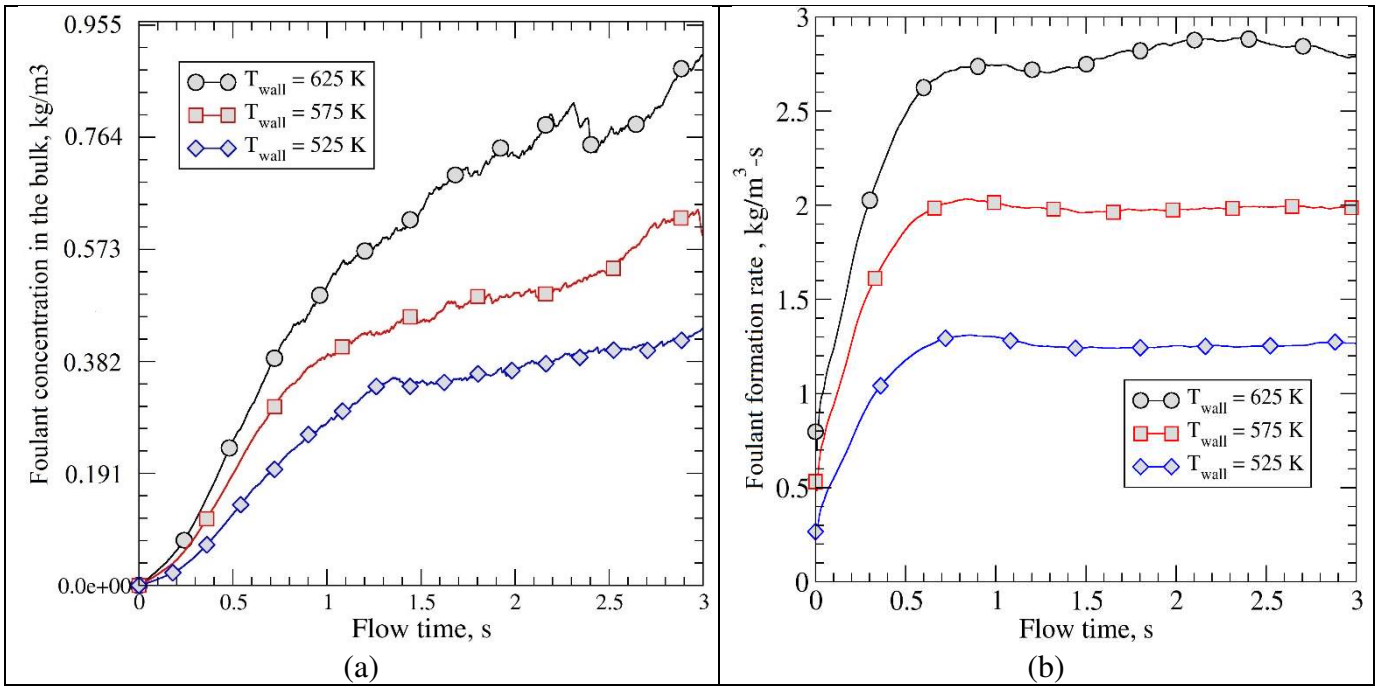

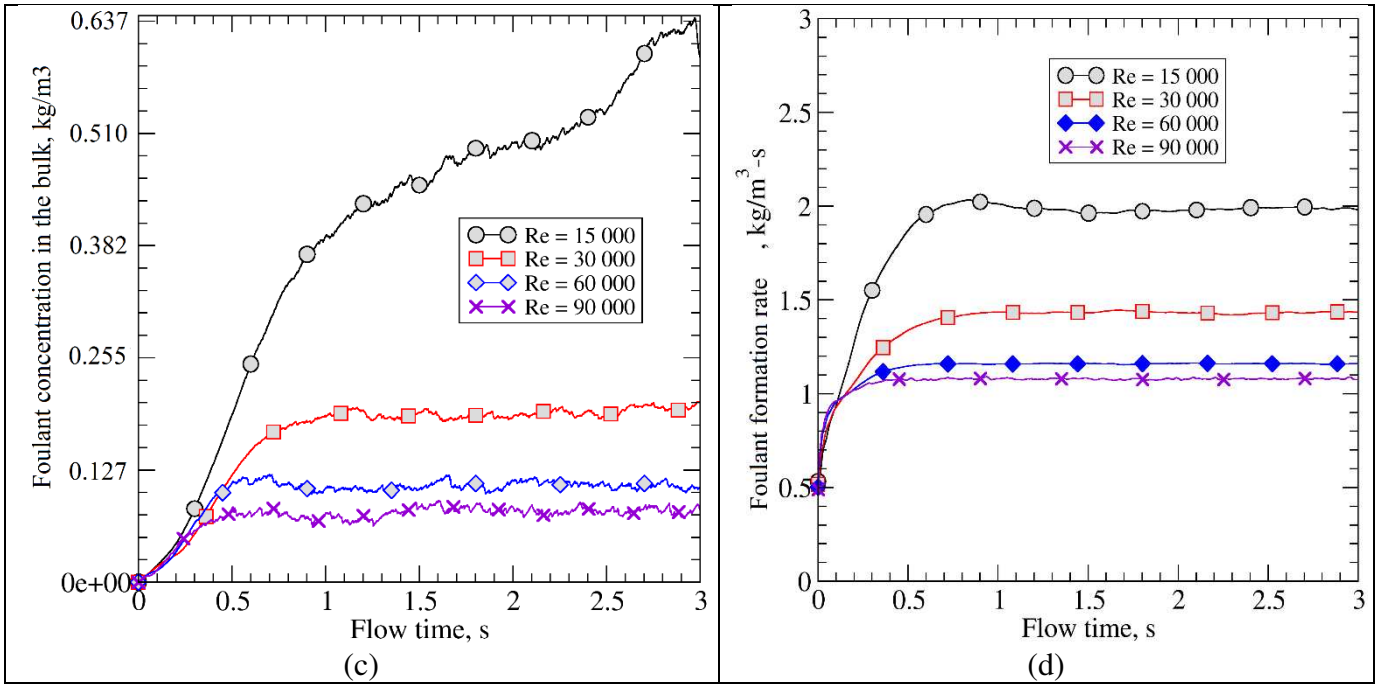

Figure 5 Effects of wall temperature and Reynolds number on the temporal evolution of foulant concentration in the bulk (a) and (c), and foulant formation rate (b) and (d).

Our previous study based on a hybrid continuum-molecular model for crude oil fouling also indicated that the chemical fouling rate rises as surface temperature increases and bulk velocity decreases in Ref. [37].

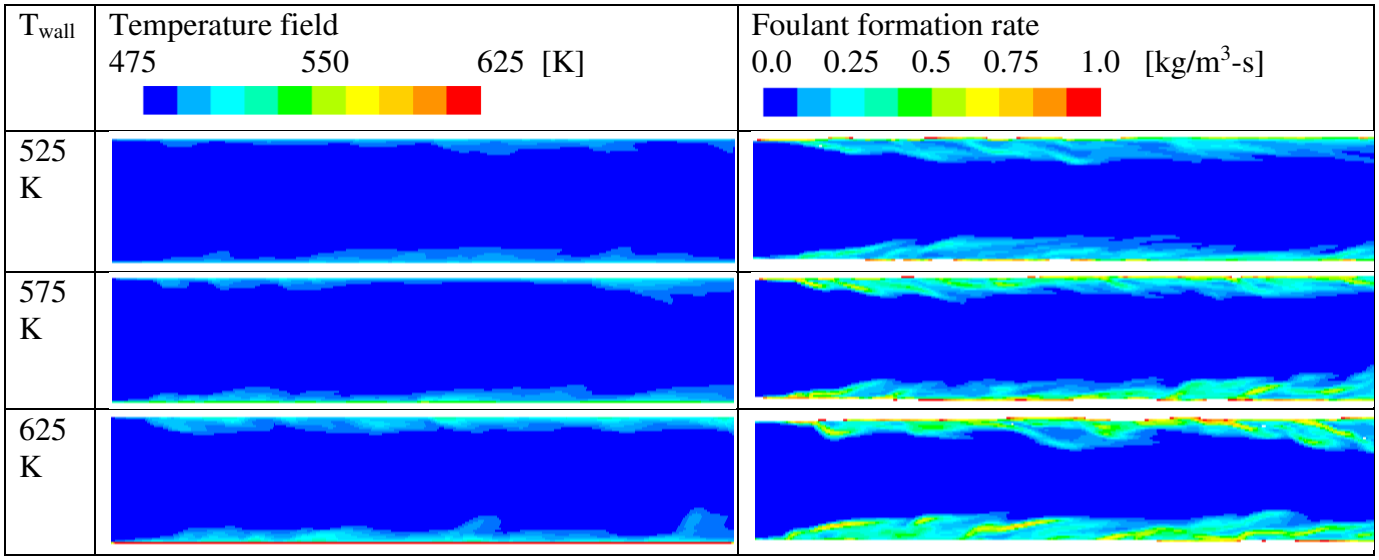

Figure 6 Instantaneous contours for temperature field and foulant formation rate under different wall temperatures with *Re* = 15000 at t = 3 s, plots were foreshortened in horizontal direction for a better view.

3.2 Analysis of Interplay Between Fouling Routes

To obtain in-depth insights into the interplay between different fouling mechanisms, the chemical fouling route and precipitation route have been activated simultaneously during the CFD simulation. The volume-averaged formation rate driven by the chemical fouling route and asphaltenes precipitation route were extracted separately. To evaluate the relative importance of the chemical fouling route, the precipitation route, and fouling removal, the ratio of chemical fouling rate to the removal rate, R_1, and the ratio of chemical fouling rate to the precipitation rate, R_2, are defined as:

$$R_1 = \frac{\text{chemical fouling rate}}{\text{removal rate}} \tag{29}$$

$$R_2 = \frac{\text{chemical fouling rate}}{\text{precipitation rate}} \tag{30}$$

Here, the volume-averaged reaction rate r_2 (see Eq. (24)) was taken as the chemical fouling formation rate, and the foulant mass flow rate through the outlet was defined as the fouling removal rate. Low R_1 values (< 1) indicate that the removal rate exceeds the formation rate, and thus that the modelled system tends to remain clean.

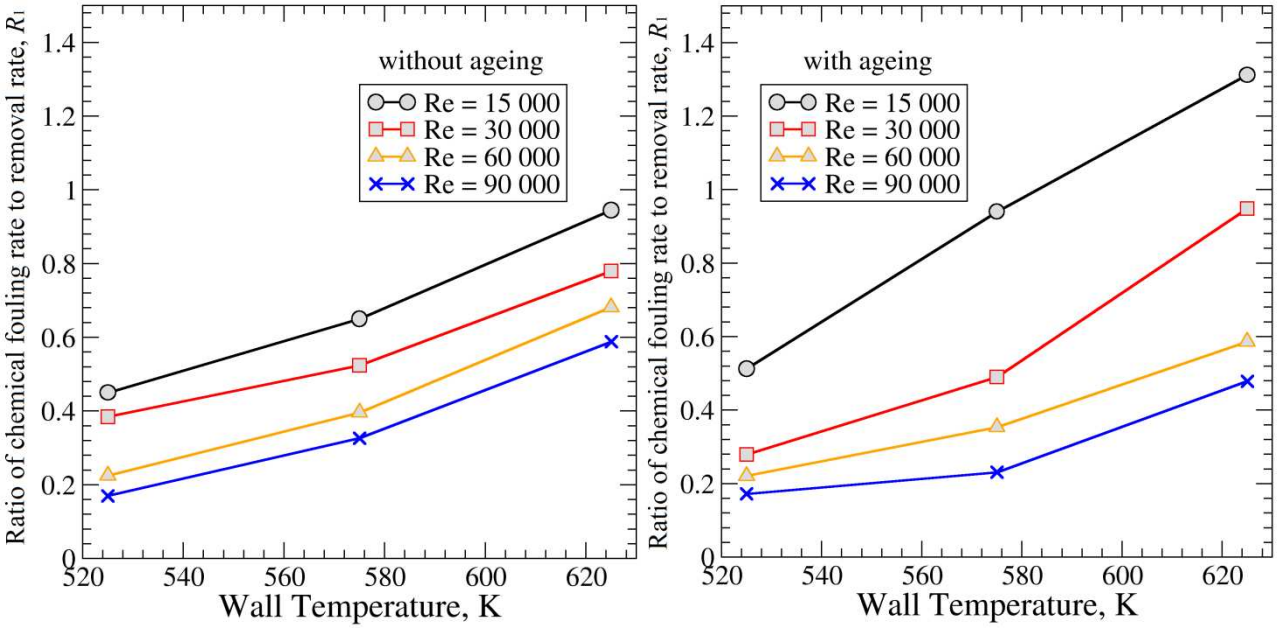

Figure 7 Ratio of chemical fouling rate to removal rate, R_1, for indicated operating conditions without (a) and with (b) ageing effects.

Figure 7 displays the variation of R_1 with wall temperature with a parametrically-varying *Re*. Values of R_1 larger than unity indicate that more foulant is produced than removed, leading to fouling accumulation in the tube. As shown in Figure 7, in the absence (presence) of ageing, R_1 remains (below) (above) unity, increases monotonically with wall temperature, and decreases with *Re*. This

can be explained by the fact that the higher wall temperatures result in higher bulk fluid temperatures, and hence faster chemical reaction rates; raising the levels of turbulence in the flow by increasing *Re*, however, leads to an acceleration of the fouling removal rate. Furthermore, fouling layers become increasingly viscous as they age, and thus more resistant to removal by bulk shear flow. This effect becomes particularly significant at high wall temperatures and low *Re*. For conditions characterized by low wall temperature and high *Re*, ageing does not affect R_1 because foulants flow out of the domain before they can undergo aging.

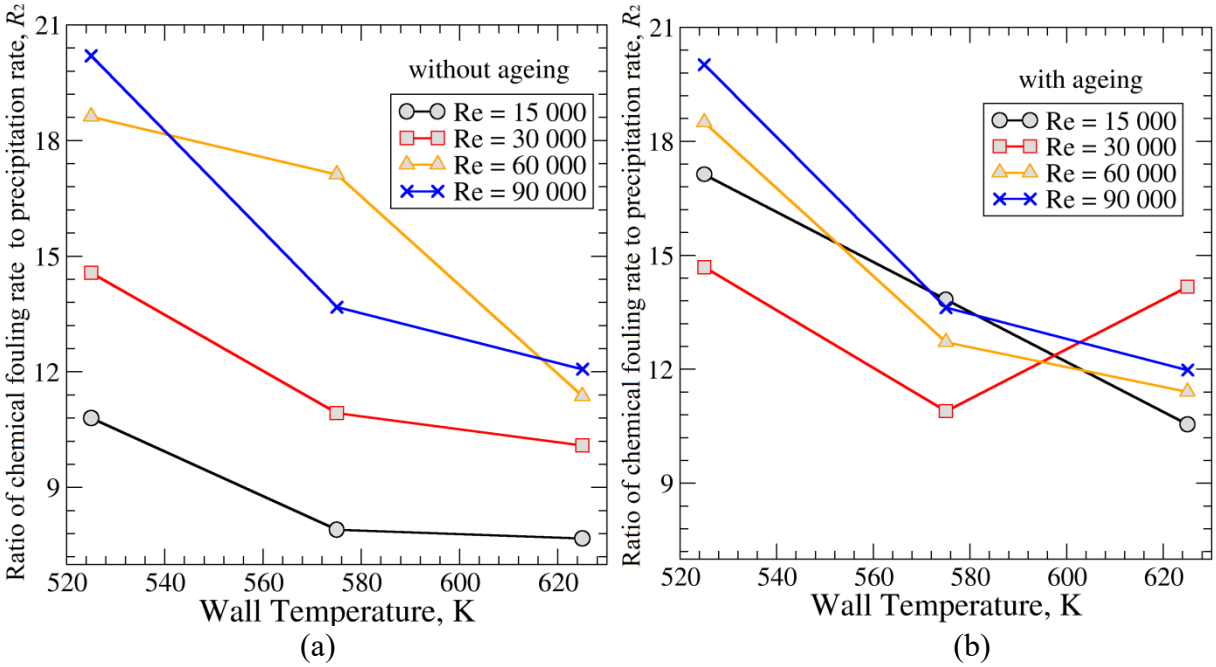

Figure 8 Ratio of chemical fouling rate to precipitation rate, R_2, for indicated operating conditions without (a) and with (b) ageing effect.

Figure 8 shows predicted values for R_2, which indicates the relative importance of chemical and precipitation fouling under various conditions. As can be seen, the R_2 values are quite large (> 8), implying that chemical fouling predominates, as also shown by the absolute formation rates via the two routes in Figure 9. The foulant formation rates driven by precipitation and chemical reaction range from 0.8 to 2.2 kg/m^3-s, and from 12 to 25 kg/m^3-s respectively at a *Re* number of 15000 without ageing.

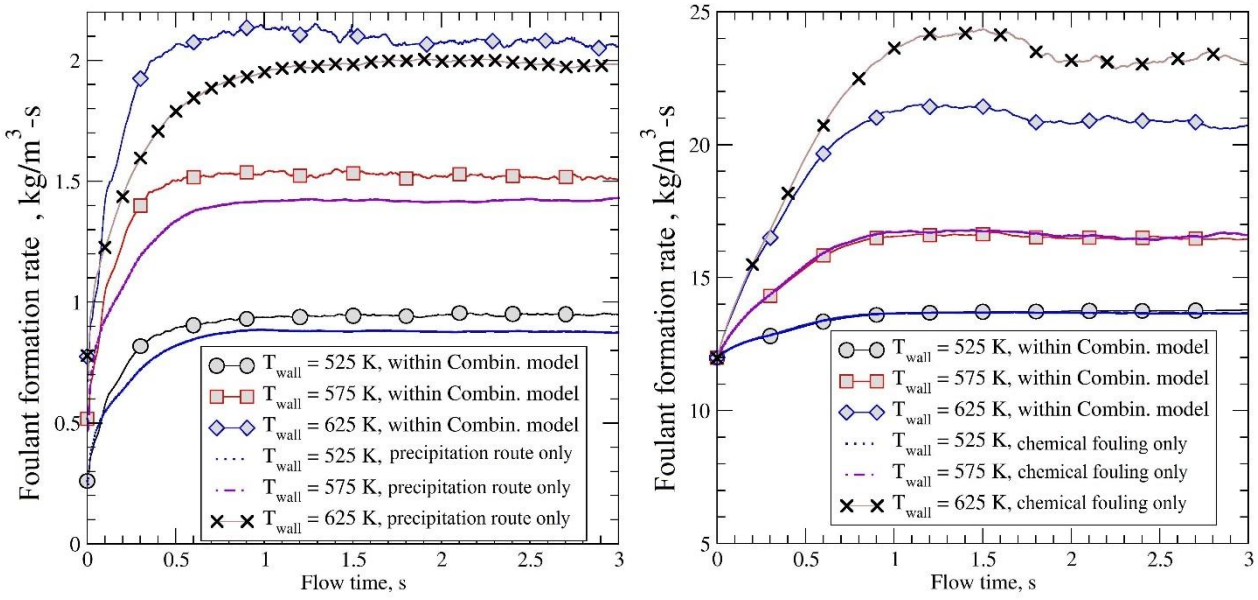

(a) (b)

Figure 9 Time courses of rates of fouling via (a) precipitation and (b) chemical reactions at indicated temperatures and *Re* 15000, without ageing.

Unlike R_1 values, the R_2 values decrease as wall temperature increases, and monotonically increase as the *Re* number increases. Increasing wall temperature also accelerates both chemical and precipitation fouling. As shown in Figure 9, for example, from 525 to 575 K the precipitation fouling rate increased almost 75%, from 0.8 to 1.4 kg/m^{3}s, while the chemical fouling rate increased only by 18%. This reflects a steep decline in the R_2 value within the corresponding temperature range. At a higher temperature range but over the same interval, 575 to 625 K, the precipitation and chemical fouling rates increased by 43% and 40%, respectively, reflecting a rather meagre decline in the value of R_2. Thus, the precipitation mechanism seems to be more sensitive than chemical fouling to temperature variation in a relative lower temperature range 525-575 K, while chemical fouling becomes sensitive to temperature variations over relative higher temperature range 575-625 K.

Turbulence has a complex effect on R_2. Generally, highly turbulent bulk flow strengthens the convective heat transfer between the hot solid wall and the cooler fluid in the core. Thus, the fluid reaches a higher temperature at thermal equilibrium. However, the highly turbulent flows also have a relatively low residence time in the tube, which is not sufficiently long to establish thermal equilibrium with the walls. Hence, at high *Re*, the bulk flow remains at a lower temperature than the walls, largely suppressing precipitation and resulting in high R_2 values.

Regarding the ageing effect, the difference in R_2 values between ageing and non-ageing conditions are minor (see data obtained for flows with *Re* numbers of 60000 and 90000 in Figs. 9(a) and (b)) in high *Re* number flows. For low *Re* numbers (*Re* = 15000 and 30000), the R_2 values increase significantly due to the high viscosity of the aged foulants.

Figure 9 also shows effects of the interactions between the precipitation and chemical fouling mechanisms. The precipitation was enhanced (Fig. 9(a)) and chemical fouling (Fig. 9(b)) suppressed in the combined model, relative to rates obtained in the respective individual model. To evaluate the degree of their mutual interaction, an "interference factor", *b*, is introduced here. This is defined as the ratio of the change in the overall foulant formation rate resulting from their interaction to the sum of fouling rates via individual routes:

$$b = \frac{\dot{m}_c - (\dot{m}_k + \dot{m}_p)}{\dot{m}_k + \dot{m}_p} \quad \textbf{(31)}$$

where $\dot{m}_c$ is the overall foulant formation rate when both mechanisms are considered simultaneously, while $\dot{m}_k$ and $\dot{m}_p$ are the predicted formation rates when precipitation or chemical fouling are considered individually. A negative *b* value indicates that suppression of chemical fouling exceeds the enhancement of precipitation fouling, so the interplay tends to reduce the overall fouling rate; a positive *b* value, on the other hand, indicates that suppression of chemical fouling is outweighed by the enhancement of precipitation. A *b* value close to zero indicates that both enhancement and suppression effects are weak, or that they effectively counterbalance each other.

The predicted interference factor, *b*, for various conditions is presented in Figure 10. Generally, negative *b* values are predicted for most conditions, except at low temperature (525 K) and high *Re* number (30000), which yield a very small positive *b* value, ~1%. As already mentioned, chemical fouling is more sensitive to temperature variations than the precipitation route. Accordingly, suppression of chemical fouling is more temperature sensitive than enhancement of precipitation. Thus, absolute *b* values increase with temperature since the suppression reduces the overall fouling rate. In addition, smaller *b* values (and larger absolute fouling rates) have been observed for flows with low *Re* numbers, suggesting that the interplay between fouling mechanisms is strengthened by reductions in turbulence. In the presence of ageing, the *b* values tend to increase. In other words, the absolute *b* values are lower than those under the same operating conditions without ageing. Thus,

ageing may either strengthen the enhancement effect or weaken the suppression effect, thereby weakening effects of the interplay on the overall fouling rate.

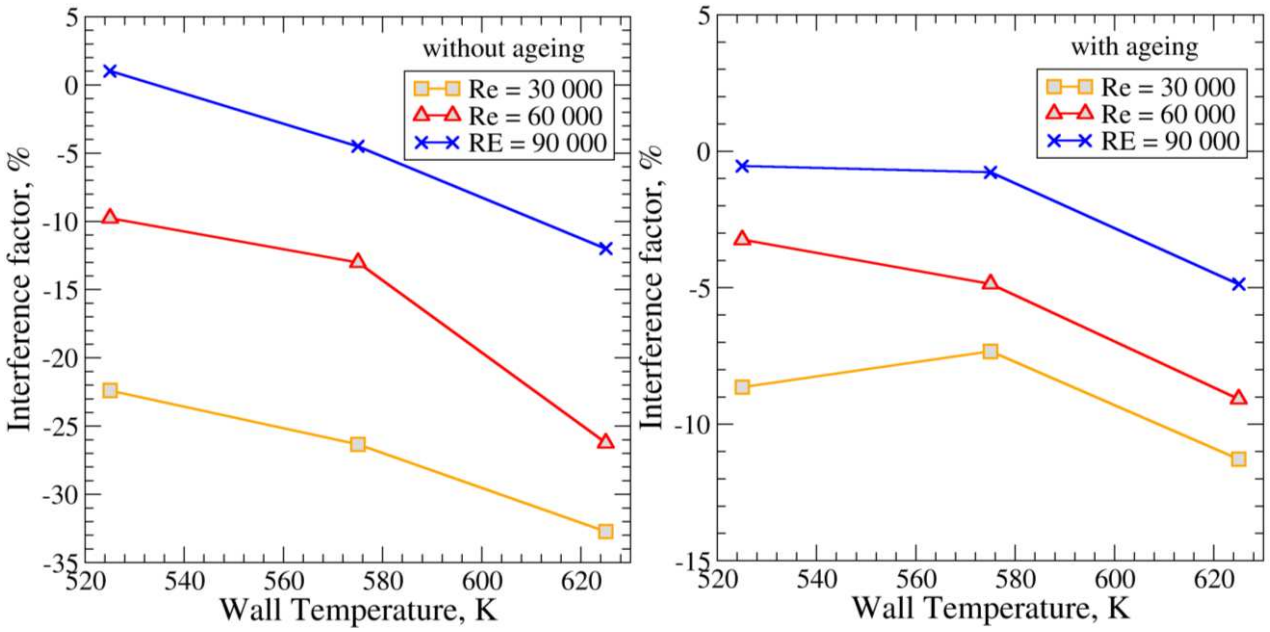

Figure 10 Predicted interference factor, *b*, for indicated conditions (a) without and (b) with ageing.

In order to understand the interplay between different fouling routes, it is necessary to elucidate the processes involved and the factors controlling them, which include the local temperature, the temperature gradient and the concentrations of both the sparingly soluble foulants and their precursors. The physical and thermal phenomena determining these local factors are:

- Interphase heat transfer: Asphaltenes precipitation induced by toluene and aromatics has been reported to be an endothermic process[60-61], hence that absorbs heat from the surroundings and reduces local temperatures, thereby suppressing chemical reactions that are governed by the temperature. In contrast, the chemical fouling reaction (two-step autoxidation scheme in Fig. 2) is exothermic[62-63], and the heat it releases will promote precipitation fouling. Thus, interphase heat transfer enhances precipitation and suppresses chemical fouling.
- Characteristics of the fouling layer. The fouling layer sticking to the wall surface weakly absorbs thermal energy and inhibits heat transfer, thus increasing temperatures adjacent to the wall and reducing temperature gradients in the bulk fluid (which enhances chemical fouling and suppresses precipitation, respectively).

- Turbulence: The turbulence generated by high speed shear flow has complex effects on fouling routes. Turbulence allows reacting species to be well mixed, thereby promoting chemical fouling, but turbulent flow leads to short residence times for reacting species, which reduce the foulant formation rate. In addition, turbulence enhances convective heat transfer and causes higher bulk temperature and small temperature gradients between wall and bulk, which promote both chemical fouling and precipitation. Moreover, the shear stress generated by turbulent flow tends to dislodge some of the fouling layer and thus enhance the removal rate.

These thermo-physical phenomena are intricately linked in most conditions and the factors are dynamic, thus predicting overall foulant formation rates is challenging. The interferential factor, b, merely presents the net outcome of these factors on the foulant formation rate. In order to identify the contribution from each process quantitatively, simulations in which effects of the interphase heat transfer, fouling layer and turbulence are isolated are needed. This is beyond the scope of the present work.

The interference factor also suggests that process modifications that slightly enhance precipitation could substantially suppress chemical fouling, which accounts for more than 90% of overall fouling, and thus reduce the total formation rate. However, manipulating individual thermo-physical processes is not trivial and usually has linked effects, e.g. increasing the local temperature enhances both chemical and precipitation fouling, while enhancing endothermic precipitation causes reductions in local temperature and suppresses chemical fouling. So, the net fouling rate depends on whether the average temperature increases or decreases, and clearly a sophisticated approach is required to isolate effects of each thermal-physical process.

3.3 Ageing Effects

As mentioned above, the ageing model including variations of molecular viscosity and thermal conductivity (Eq. (28)) affects the foulant formation rate, removal rate and interplay between fouling routes. The ageing effects on viscosity depend on the lifetimes of the foulants and shear stress generated by turbulent bulk flows. The volume-averaged molecular viscosity of foulant has therefore been plotted as a function of time for different Re numbers at a fixed wall temperature. The results

(Fig. 11(a)) show that the averaged viscosity increases gradually with flow time, indicating that microstructures (e.g. polyaromatic- or graphitic-like structures[64]) evolve correspondingly in the foulant layer. Meanwhile, the fast moving bulk oil (which has a large *Re* number) generates higher shear stress above the fouling layer, which degrades the age-related microstructures, resulting in a relatively low viscosity in the top region of the fouling layer. The averaged foulant viscosity peaks when the competition between structuration and destructuration is in equilibrium. The viscosity increases by 2% to 17% with ageing depending on the *Re* number, in the *Re* number range from 90000 to 15000.

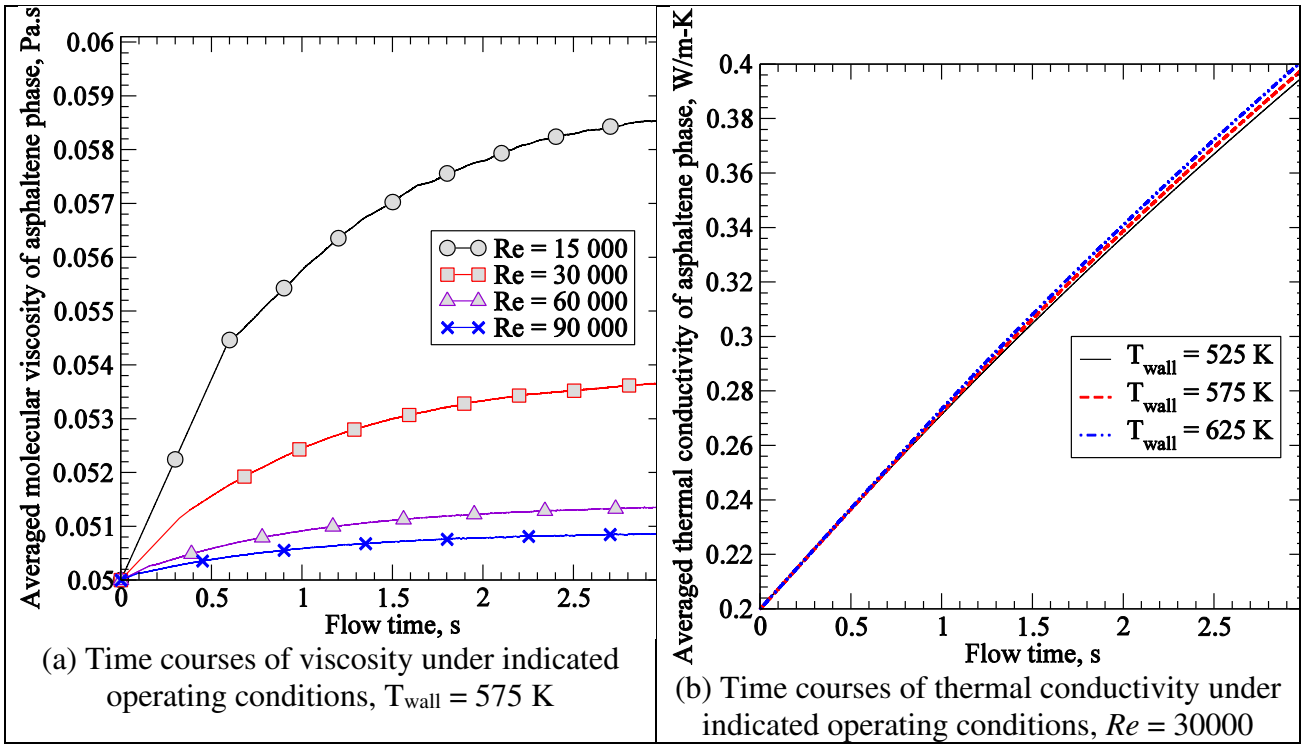

(a) Time courses of viscosity under indicated operating conditions, T_{wall} = 575 K

(b) Time courses of thermal conductivity under indicated operating conditions, *Re* = 30000

Figure 11 The ageing effect on volume-averaged properties of foulants: a) molecular viscosity and b) thermal conductivity, under indicated conditions.

Figure 11(b) shows that the averaged thermal conductivity increases linearly as a function of time at various wall temperatures and a fixed bulk flow velocity. By the end of the simulation it has only increased two-fold. Furthermore, ageing effects of thermal conductivity seem to be insensitive to the temperature: only a small deviation (< 1%) in the variable has been observed across the temperature range of 525 K – 625 K. The variation of viscosity and thermal conductivity due to ageing directly affects foulant removal and formation rates, which in turn influence the R_1, R_2 and b values, as discussed in the previous section.

The present work presents a first attempt at quantitatively evaluating the interaction between fouling routes and the impact of ageing. Limitations of the numerical results are the short timescale (only 3 seconds flow time) and the lack of experimental validation. The industrial heat exchanger network needs much longer time to reach thermal steady state. Given sufficient **computing** resources, the current model could achieve a longer timespan (minutes or hours) and provide valuable insights into the fouling process. On the other hand, the induction period of lab scale fouling rig is relatively short. Experimental data from such rigs, e.g. High Pressure Oil Rig (HIPOR)[65], would be very valuable for validating the current model.

4. Conclusion

A fouling model including foulant formation and ageing has been implemented in a CFD code to better understand the induction period (up to three seconds flow time) of fouling processes in a tube heat exchanger. The effects of varying the wall temperature and bulk flow velocity on the foulant formation rate, removal rate and ageing process have been examined in a set of CFD simulations with various operating conditions. The foulant concentration and averaged foulant formation rates via different routes have been predicted and compared. As expected, increasing the wall surface temperature accelerated the foulant formation rate and increased the foulant concentration. Increasing the bulk velocity (and thus *Re* numbers) decreased the fouling and removal rates, and resulted in lower foulant concentration in the heat exchanger.

To evaluate the relative importance of fouling routes, two dimensionless constants, R_1 and R_2, were used to probe shifts in ratios of the chemical fouling rate to removal rate, and chemical fouling rate to precipitation rate, respectively. R_1 values increase as the surface temperature increases, and decrease as the *Re* number increases. Therefore, the optimal operating conditions for heat exchangers to minimize fouling include low temperature and high *Re* numbers. The predicted R_2 values are quite large (>8 for all considered cases), suggesting that chemical fouling greatly exceeds precipitation-based fouling, but decrease as temperature increases, and increase as *Re* numbers increase. In addition, chemical fouling is suppressed and precipitation enhanced when these routes are combined.

To assess the interplay between these fouling routes, an interference factor, *b*, was introduced. Three possible driving forces (interphase heat transfer, inhibition of heat transfer in the fouling layer and turbulence) were identified that may either strengthen or weaken the processes. Furthermore, by strengthening or weakening these driving forces appropriately, the chemical fouling rate could be substantially reduced while only slightly increasing the precipitation rate. However, these driving forces are intricately linked, and manipulating them individually is not trivial. Therefore, a sophisticated approach is needed to weigh the quantitative effects of each driving force on the interactions.

Regarding ageing effects, the time courses of the foulants' viscosity and thermal conductivity have also been plotted and compared under different operating conditions. The viscosity appears to be quite sensitive to the *Re* number, which governs the degradation of age-related microstructures. The temperature affects the thermal conductivity mildly. However, both viscosity and thermal conductivity increase as foulant ages. In addition, the ageing process significantly increases the R_1 values under high temperature and low *Re* number conditions, but increases the R_2 values under low temperature and low *Re* number conditions. Under other conditions, the impact of ageing on R_1 and R_2 is minor. The ageing effect weakens the interference factor, hence the offset between suppression and enhancement is larger with than without ageing.

Acknowledgments

This research was performed under the UNIHEAT project. The authors wish to acknowledge the Skolkovo Foundation and BP for financial support. The author is also grateful to Professor Omar Matar for useful discussions.

References

1. Epstein N. Thinking about heat transfer fouling: A 5X5 matrix. *Heat Transfer Engineering*. 1981:4(1):43-56.
2. Wilson DI, Ishiyama EM, Paterson WR, Watkinson AP. Ageing: looking back and looking forward. In: Proceedings of International Conference on Heat Exchanger Fouling and Cleaning VIII, Schladming, Austria, 2009.

3. Deshannavar UB, Rafeen MS, Ramasamy M, Subbarao D. Crude oil fouling: A review. *J. Applied Sci.* 2010;10:3167-3174.
4. Kern KQ, Seaton RE. A theoretical analysis of thermal surface fouling. *British Chemical Engineering*. 1959;4(5):258-262.
5. Crittenden B, Kolaczkowski S. Mass transfer and chemical kinetics in hydrocarbon fouling. In: Proceedings of the Conference on Fouling Science or Art, London, UK, 1979.
6. Crittenden BD, Kolaczkowski ST, Hout SA. Modelling hydrocarbon fouling. *Trans. Chem. Part A*. 1987;65:171-179.
7. Epstein N. A model of the initial chemical reaction fouling rate for flow within a heated tube and its verification. *Int. Institution of Chemical Engineers Symposium Series*. Hemisphere Publishing Corporation. 1994;135-225.
8. Yeap B, Wilson D, Polley G, Pugh S. Mitigation of crude oil refinery heat exchanger fouling through retrofits based on thermo-hydraulic fouling models. *Chemical Engineering Research and Design*. 2004;82(1):53 -71.
9. Ebert W, Panchal CB. Analysis of exxon crude-oil-slip stream coking data. Technical report. Argonne National Lab. United States. 1995.
10. Polley GT, Wilson DI, Yeap BL, Pugh SJ. Evaluation of laboratory crude oil threshold fouling data for application to refinery pre-heat trains. *Applied Thermal Engineering*. 2002;22(7):777-788.
11. Nasr MRJ, Givi MM. Modeling of crude oil fouling in preheat exchangers of refinery distillation units. *Applied thermal engineering*. 2006;26(14):1572-1577.
12. Shetty N, Deshannavar UB, Gounder R, Pendyala R. Improved threshold fouling models for crude oils. *Energy*. 2016;111:453-467.
13. Aminian J, Shahhosseini S. Evaluation of ANN modeling for prediction of crude oil fouling behaviour. *Applied Thermal Engineering*. 2008;28:668–674.
14. Coletti F, Macchietto S, Polley GT. Effects of fouling on performance of retrofitted heat exchanger networks: A thermo-hydraulic based analysis. *Computers & Chemical Engineering*. 2011;35(5):907-917.
15. Ménard T, Tanguy S, Berlemont A. Coupling level set/VOF/ghost fluid methods: Validation and application to 3D simulation of the primary break-up of a liquid jet. *Int. J. Multiphase Flow*. 2007;33:510–524.
16. Sileri D, Sahu K, Ding H, Matar OK. Mathematical modelling of asphaltenes deposition and removal in crude distillation units. In: Proceedings of International Conference on Heat Exchanger Fouling and Cleaning VIII, Schladming, Austria, 2009.
17. Bayat M, Aminian J, Bazmi M, Shahhosseini S, Sharifi K. CFD modeling of fouling in crude oil pre-heaters. *Energy Conversion and Management*. 2012;64:344-350.
18. Tavakkoli M, He P, Lin PH, Rezaee S, Puerto M, Doherty R, Creek J, Wang J, Kusinski G, Gomes J, Chapman W, Biswal SL, Vargas, FM. Asphaltene Deposition and Fouling in Reservoirs. Offshore Technology Conference, Paper No. OTC-27933-MS, Huston, USA, 2017.
19. Loyola-Fuentes J, Jobson M, Smith R. Fouling modelling and mitigation for crude oil heat exchanger networks using reconciled operating data. *Journal Chemical Engineering Transactions*, 2018;70:193-198.
20. Emani S, Gounder RM, Shaari KZK. Discrete Phase-CFD Simulations of Asphaltenes Particles Deposition from Crude oil in Shell and Tube Heat Exchangers. *Applied Thermal Engineering.* 2019;149:105-118.

21. Maddahian R, Farsani AT, Ghorbani M. Numerical investigation of asphaltene fouling growth in crude oil preheat trains using multi-fluid approach. *Journal of Petroleum Science and Engineering*. 2020;188. Paper No.106879.
22. Rammerstorfer E, Karner T, Siebenhofer M. The kinetics and mechanisms of fouling in crude oil heat transfer. *Heat Transfer Engineering*. 2020;41(8):691-707.
23. Ishiyama E, Pugh S, Wilson I. Incorporating Deposit Ageing into Visualisation of Crude Oil Preheat Train Fouling. *Process Integration and Optimization for Sustainability*. ISSN 2509-4238, Springer Nature, 2020.
24. Wilson DI, Polley GT, Pugh SJ. Ten years of Ebert, Panchal and the 'Threshold Fouling Concept'. *Proc. 6th International Conference on Heat Exchanger Fouling and Cleaning: Challenge and Opportunities*. Eds. H. Müller -Steinhagen, M. Reza Malayeri and A. P. Watkinson, Engineering Conferences International, Kloster Irsee, Germany, 2005, pp. 25-36
25. Coletti F, Crittenden BD, Macchietto S. Basic Science of Fouling Process. In: *Crude Oil Fouling: Deposition Characterization, Measurements*. Coletti F, Hewitt GF (Eds.): Elsevier, 2014;37.
26. Groysman A. Corrosion Problems and Solutions in Oil Refining and Petrochemical Industry, Chapter 7, Fouling, Corrosion and Cleaning, Spinger, 2017;218.
27. Phillips D. Z. Mitigation of crude oil fouling by the use of HiTRAN inserts. PhD thesis, University of Bath, 2000;14.
28. Yang M, Young A, Niyetkaliyev A, Crittenden B. Modelling fouling induction periods. *International Journal of Thermal Sciences*, 2012;51:175-183.
29. Yang J, Matar OK, Hewitt GF, Zheng W, Manchanda P. Modeling of Fundamental transfer Processes in Crude-oil Fouling. In: Proceeding of 15th International Heat Transfer Conference (IHTC-15), Kyoto, Japan, 2014.
30. Yang J, Sileri D, Matar OK. Fundamental transport modelling. In: *Crude Oil Fouling: Deposition Characterization, Measurements*. Coletti F, Hewitt GF (Eds.): Elsevier, 2014;242:284.
31. Faghri A, Howell JR, Zhang Y. Chapter 2: Generalized Governing Equation for Heat and Mass Transfer, in: Advanced Heat and Mass Transfer, Global Digital Press, 2010.
32. Brackbill JU, Kothe DB, Zemach C. A Continuum Method for Modeling Surface Tension. *J. Comput. Phys.* 1992;100:335-354.
33. Smagorinsky J. General Circulation Experiments with the Primitive Equations I. The Basic Experiment. *Month. Wea. Rev.* 1963;91:99-164.
34. ANSYS®Academic Research, Release 18.0, Help System, *ANSYS FLUENT Manual,* ANSYS, Inc., 2018.
35. Jewell DM, Weber JH, Bunger JW, Plancher H, Latham DR. Ion-exchange, coordination and adsorption chromatographic separation of heavy-end petroleum distillates. *Anal. Chem.* 1972;44:1391-1395.
36. Miquel J, Hernandez J, Castells F. A new method for petroleum fractions and crude oil characterization. *SPE Reserv. Eng.* 1992;265–270.
37. Yang J, Jimenez-Serratos MG, Fari-Arole DS, Müller EA, Matar OK. Crude Oil Fouling: Fluid Dynamics, Reactions and Phase Change. In: Proceeding of IUTAM Symposium on Multiphase Flows with Phase Change Challenges and Opportunities, Hyderabad, India, 2014.
38. Watkinson AP, Wilson DI. Chemical reaction fouling: A review. *Experimental Thermal and Fluid Science*. 1997:14 (4):361-374.
39. Buenrostro-Gonzalez E, Lira-Galeana C, Gil-Villegas A, Wu, JZ. Asphaltene precipitation in crude oils: Theory and experiments. *AIChE J*. 2004;50:2552–2570

40. Panchal CB, Watkinson AP. Chemical reaction fouling model for single-phase heat transfer. Technical report, Argonne National Lab., United States, 1993.
41. Russell GA. Oxidation of Unsaturated Compounds. III. Products of the Reaction of Indene and Oxygen; Stereochemistry of the Addition of a Peroxy Radical and Oxygen to a Double Bond. *J. Am. Chem. Soc.* 1956;79:1035-1040.
42. Crittenden BD, Khater EMH. Fouling From Vaporizing Kerosine. *Journal of Heat Transfer.* 1987;109:583–589.
43. Domke CH, Davison RR, Glover CJ. Effect of Oxygen pressure on asphalt oxidation kinetics. *Ind. Eng. Chem. Res.* 2000;39:592–598.
44. Lambourn GA, Durrieu M, Hewitt I, Afghan T. Fouling in Crude Oil Preheat Trains. In: *Heat Exchangers: Theory and Practice*. Taborek J, Hewitt GF, Afgan NH.(Eds.). McGraw-Hill, New York, USA, ISBN: 9780070628069, 1983;841-852.
45. Hong E, Watkinson P. A study of asphaltene solubility and precipitation. *Fuel*. 2004;83:1881–1887.
46. Spiecker PM, Gawrys KL, Kilpatrick PK. Aggregation and solubility behavior of asphaltenes and their subfractions. *J. Colloid Interface Sci.* 2003;267:178–193.
47. Maqbool T, Srikiratiwong P, Fogler HS. Effect of temperature on the precipitation kinetics of asphaltenes. *Energy & Fuels*. 2011;25:694–700.
48. Wu J, Prausnitz JM, Firoozabadi A. Molecular–Thermodynamic Framework for Asphaltene–Oil Equilibria. *AIChE J.* 1998;44:1188.
49. Artola PA, Pereira FE, Adjiman CS, Galindo A, Muller EA, Jackson G, Haslam AJ. Understanding the fluid phase behaviour of crude oil: Asphaltene precipitation. *Fluid Phase Equilibra.* 2011;306:129-136.
50. Cooper S. *Course Notes*, Department of Chemistry, University of Durham, England (http://www.dur.ac.uk/sharon.cooper/lectures/colloids/interfacesweb1.html), 2005.
51. Svendsen JA. Mathematical-modeling of wax deposition in oil pipeline systems. *AIChE Journal*. 1993;39(8):1377–1388.
52. Duran JA, Schoeggl FF, Yarranton HW. Kinetics of Asphaltene Precipitation/Aggregation from Diluted Crude Oil. *Fuel*. 2019;255,115859.
53. McGarvey GB, Turner CW. Synergism models for heat exchanger fouling mitigation Understanding Heat Exchanger Fouling and Its Mitigation, *Engineering Foundation Conf*, Italy (1997).
54. Shen C, Wang Y, Tang Z, Yao Y, Huang Y, Wang X. Experimental study on the interaction between particulate fouling and precipitation fouling in the fouling process on heat transfer tubes. *Int. J. Heat Mass Tran.* 2019;138:1238-1250.
55. Zhu T, Dittrich M. Carbonate Precipitation through Microbial Activities in Natural Environment, and Their Potential in Biotechnology: A Review. *Front Bioeng Biotechnol*. 2016;4:4.
56. Schoenitz M, Grundemann L, Augustin W, Scholl S. Fouling in microstructured devices: a review. *Chem. Commun*. 2015;51:8213-8228.
57. Coussot P. Rheophysics of pastes: a review of microscopic modelling approaches. *Soft Matter*. 2007;3(5):528-540.
58. Ishiyama EM, Paterson WR, Wilson DI. The effect of fouling on heat transfer, pressure drop, and throughput in refinery preheat trains: Optimization of cleaning schedules. *Heat Transfer Engineering*. 2009;30(10-11):805-814.
59. ANSYS®Academic Research, Release 18.0, Help System, *ANSYS ICEMCFD Manual*, ANSYS, Inc., 2018.

60. Andersen SI, Birdi KS. Aggregation of asphaltenes as determined by calorimetry. *J. Coll. Int. Sci.* 1991;142:497-502.
61. Andersen SI, Christensen SD. The critical micelle concentration of asphaltenes as measured by calorimetry. *Energy&Fuel*. 2000;14:38-42.
62. Coletti F, Hewitt G. *Crude Oil Fouling, Deposit Characterization, Measurements, and Modeling*, Gulf Professional Publishing, 2014;28.
63. Wilson DI, Watkinson AP. A study of autoxidation reaction fouling in heat exchangers. *Can. J. Chem. Eng.* 1996;74(2):236– 246.
64. Fan Z, Watkinson AP. Kinetics and structural evolution during aging of coker vapor deposits. *Heat Transfer Engineering*. 2011;32(3-4):237-247.
65. Tajudin Z, Martinez Minuesa J, Diaz-Bejarano E, Valkov I, Orzlowski P, Coletti F, Macchietto S, Hewitt G. Experiment Analysis and Baseline Hydraulic Characterisation of HiPOR, a High Pressure Crude Oil Fouling Rig. *Chemical Engineering Transactions*. 2015:43:1405-1410.